buildings

MDPI

Article

Optimisation of Sunflower Husk Ash-Activated Slag Binder

Olivera Bedov [1,2], Suzana Draganić [1,*], Snežana Vučetić [3] and Marijana Serdar [2]

[1] University of Novi Sad, Faculty of Technical Sciences, Department of Civil Engineering and Geodesy, 21000 Novi Sad, Serbia; olivera.bukvic@uns.ac.rs
[2] University of Zagreb, Faculty of Civil Engineering, Department of Materials, 10000 Zagreb, Croatia; marijana.serdar@grad.unizg.hr
[3] University of Novi Sad, Faculty of Technology, Department of Materials Engineering, 21000 Novi Sad, Serbia; snezanap@uns.ac.rs
* Correspondence: suzanav@uns.ac.rs

Abstract

This study presents the optimisation of an alkali-activated binder produced from ground granulated blast furnace slag (GGBFS) and potassium-rich sunflower husk ash (SHA), by varying SHA content, curing regime, and mixing procedure. Both materials are locally available in the Republic of Serbia. The influence of SHA content (15%, 25%, and 35% by mass of GGBFS) and curing conditions (ambient and 65 °C) on hydration products, workability, and compressive strength was examined. The water-to-binder ratio and GGBFS content were kept constant, and a one-part alkali activation approach was employed using untreated SHA. Fourier-transform infrared spectroscopy (FTIR) and thermogravimetric analysis (TGA) were performed on paste samples, after 2, 7 and 28 days of curing, while workability and compressive strength of mortars were measured after 7 and 28 days. Increasing SHA content enhanced the formation of C-S-H and C-A-S-H gels, resulting in a consistent rise in compressive strength, from 26.6 MPa to 36.2 MPa after 7 days and from 46.2 MPa to 55.1 MPa after 28 days of ambient curing. Workability was slightly reduced with increasing SHA content, resulting in flow diameters of 156.04 mm (15% SHA), 154.10 mm (25% SHA) and 152.76 mm (35% SHA). Curing at 65 °C accelerated early strength gain for 33% to 39% but produced lower 28-day strengths than ambient curing. Additionally, for the optimal mix, SHA was also pre-immersed in water for varying durations to assess its effect on workability, compressive strength, and potassium ion leaching. This pretreatment increased compressive strength by up to 14.7%, depending on immersion time, but reduced workability by up to 15.5%. The novelty of the research is reflected in attaining the highest 28-day compressive strength of 55 MPa (for 25% SHA by mass of GGBFS), under ambient curing, without SHA pretreatment or immersion, highlighting the potential for low-energy, sustainable binder systems using agricultural and industrial by-products.

Keywords: alternative binders; alkali-activated materials; alternative activator; biomass ash; sunflower husk ash; valorisation; one-part alkali-activation

check for updates

Academic Editor: Yichao Zhang

Received: 31 October 2025
Revised: 16 November 2025
Accepted: 18 November 2025
Published: 21 November 2025

Citation: Bedov, O.; Draganić, S.; Vučetić, S.; Serdar, M. Optimisation of Sunflower Husk Ash-Activated Slag Binder. *Buildings* **2025**, *15*, 4210. https://doi.org/10.3390/buildings15234210

Copyright: © 2025 by the authors. Licensee MDPI, Basel, Switzerland. This article is an open access article distributed under the terms and conditions of the Creative Commons Attribution (CC BY) license (https://creativecommons.org/licenses/by/4.0/).

1. Introduction

Decarbonisation of the construction industry is one of the primary strategies for achieving the global goal of net-zero carbon dioxide emissions by 2050 [1]. Changes in the cement industry are necessary to achieve this goal, as cement is used to produce concrete, the most widely used construction material, and is responsible for approximately 7% of anthropogenic CO_2 emissions [2]. Given the data on cement production rates being

comparable to global food production, and the global increase in urbanisation [3], several pathways toward sustainable concrete have been proposed [1,2], including the development of alternative binders.

Alkali-activated materials (AAMs) are binders synthesised from aluminosilicate precursors and alkaline activators. The most common precursors are coal fly ash (FA), blast furnace slag (BFS), and calcined clays or metakaolin (MK). Alkaline activators are usually potassium or sodium hydroxides and silicates, while carbonates and sulphates can also be used, depending on the type of precursor [4]. Activators initiate and catalyse the dissolution of Si and Al from the precursors, allowing for their polymerisation and the formation of a binding structure [5]. The justification for AAM's application lies in the reduction of CO_2 emissions by avoiding the use of cement and utilising waste materials [6]. A well-designed AAMs mix can significantly reduce the CO_2 emissions compared to Portland cement (PC) concrete production, depending on the type and availability of used precursors and activators [7]. A study on the environmental impact of alkali-activated concretes with different precursors [8] showed that BFS-based alkali-activated concrete has 57%, FA-based 42%, and MK-based concrete has 39% lower CO_2 emissions, compared to PC concrete. Furthermore, their performance can match or even surpass that of PC concrete. Therefore, interest in AAMs is being renewed, although alkali-activation has been extensively researched and applied on a large scale at varying degrees since the 1950s [6]. However, the variety of component materials implies a wide range of properties, as well as a diversity in supply chains [4,9]. Along with the technological problems and lack of regulations [4], AAMs are hindered from achieving a wide and unified application [9].

The environmental challenge of the AAMs is the inevitable presence of synthetic chemical activators, resulting from CO_2 emissions and energy consumption, as well as ozone layer depletion and ecotoxicity [5,8]. Their high cost and safety issues associated with handling the highly caustic activator solution additionally limit the widespread application of AAMs in the construction sector [10,11]. Hence, replacing conventional chemical activators with waste-derived silica and alkali-rich alternatives that exhibit comparable performance became a research interest [12]. Industrial by-products investigated as a replacement for silicate activators are silica fume and glass waste [13,14], while red mud is proposed as an alkali source [13]. Biomass ashes are also considered as a promising alternative activators, since they are rich in potassium, calcium and amorphous silica, depending on the type of plant they originate from [15]. Worldwide, biomass-fired power plants produce 480 million tonnes of ash per year [16] and it is estimated that biomass as an alternative energy source could replace 33–50% of the global energy deposit by 2050 [17]. Some biomass ashes can have different applications across industries, such as supplementary cementitious material (construction) or soil quality improvement as fertilisers, reclamation and remediation agents (agriculture and mining) [17]. However, a significant amount of biomass ashes is still landfilled. Besides replacing the chemical activators in AAMs, using biomass ashes can also mitigate the environmental problem of ash disposal. Potential upscaling as an alternative activator in AAM technology could be a promising pathway to achieving "no waste" circular economy goals while enhancing the sustainability of AAMs [12,18,19], since valorisation of waste materials and industrial by-products in the construction sector has been proven as a successful strategy [20].

Agricultural biomass ashes (ABA), such as rice husk ash [21–30] and sugarcane straw ash [23,24], were investigated as sources of silica for the activation of various precursors. Olive-stone biomass ash (OBA) [30–34], maize cob and stalk ash [35], cotton shell ash (CSA) [36], wood biomass ash (WBA) [37,38], almond-shell biomass ash (ASBA) [39,40], nutshell and mango biomass ash (MBA) [34], hazelnut shell ashes (HBA) [34,41], sunflower

hull (husk) ash (SHA) and sunflower stalk ash (SSA) [42–44], as well as coffee-husk ash (CHA) [45] have proven to be effective sources of potassium.

According to the literature review, ABA was identified as the most effective activator for BFS compared to other precursors (fly ash and metakaolin). The performance of these AAMs has been tested on paste and mortar samples.

The AAMs were usually mixed by one-part alkali-activation [31,32,40], i.e., without previous dissolution of ABA in water [11]. However, some authors reported using dissolved ABA for the preparation of AAMs with [30] and without [41] filtering the suspension. To the best of the author's knowledge, there are no studies on the optimal dissolution time of the ABA activator prior to mixing and its influence on the AAMs properties. Some studies reported drying and/or milling as ash pretreatments [31,32,40,41,43], while there is no research on untreated ABA in AAMs.

The chemical composition of the examined ashes revealed high contents of K_2O, e.g., 61.78% in CHA [45], 32.16% in OBA [31], 31.81% [34] and 19.88% [41] in HBA, 36.67% in SSA [44] and 21.37% in SHA [43]. Furthermore, some of the ABA analyses showed the moderate to high CaO content (12–18% in SHA and SSA [43], 27.77% in OBA [31,32]). In the published research, the ash content was usually determined as an addition (5–30%) [30,32,41] and as a partial replacement (15–35%) by mass of precursor [30,32,33]. Alternatively, ABA was added to reassemble different molarities of activator solutions [31]. A range of liquid-to-solid (l/s) ratios was used for paste formulations (0.32–0.45) [33,41]. In mortar formulations, the water-to-binder (w/b) ratio was 0.40 [32,39].

The curing regimes varied across studies, with curing temperatures in the first 24 h ranging from 20 °C to 85 °C (typically 65 °C for most studies) and durations between 4 and 48 h [31,32], followed by post-curing (after demoulding) at either ambient (18–23 °C, 55–100% RH) [31,33,41,45] or elevated (65 °C) conditions for 7 days [32,34,40]. Therefore, the reported compressive strengths are various, from 22.1 MPa at 28 days of ambient curing [41] to 45.2 MPa after 7 days of curing at 65 °C [40]. The ABA-activated AAMs exhibited comparable or superior performance to the reference mixes, which were activated with commercial KOH or NaOH [31,33,39,40,45]. For example, OBA-activated BFS paste samples resulted in compressive strength of 29 MPa after 7 days of curing and outperformed the reference mixes activated with the 4 M water solution of commercial KOH (16.9 MPa) [31].

The published research on sunflower-originated biomass ashes includes sunflower stalk ash (SSA), sunflower hull or husk ash (SHA), also denoted as sunflower shell fly ash (SSFA) [42–44,46,47]. Several papers are focused on the development of grouting slurries by activating BFS [42–44]. Grouting mixes with SSA and SHA were cured at 20 °C and 95%RH, reaching higher 28-day compressive strength than reference mixes as well (24.88 MPa—SSA, 21.27 MPa—SHA, 9.58 MPa—KOH and 11.59 MPa—NaOH) [43]. SSA was also successfully used for the activation of the BFS and black rice hull ash grouts [42]. The obtained results met the requirements of grouting engineering [42], with SSA-activated samples demonstrating significantly higher compressive strength compared to the samples activated with conventional activators (KOH, NaOH). The same group of authors tested changes in setting time and workability of the slurries [42,43], as well as microstructure by X-ray diffraction (XRD) [42–44] and pore structure by mercury intrusion porosimetry [44]. The analysis of heavy metal leaching from slurries after 28 days of curing indicated that formed hydration products can promote the immobilisation of heavy metals with the formed C–(A)–S–H gel [42].

SSFA was also used to produce paste samples by activating ladle slag in the research of Nikolov et al. [47]. The results showed that the compressive strength of 30 MPa can be

achieved by adding 10% of SSFA, by mass of ladle slag, while higher contents resulted in a decrease in compressive strength.

The main goal of this study is to optimise the performance and mixing process of a fully waste-based alkali-activated binder, based on potassium-rich SHA as an alternative alkali hydroxide activator and ground granulated blast furnace slag (GGBFS) as the precursor. GGBFS originates from the iron and steel production company in the Republic of Serbia, where the annual pig iron production in 2022 was 1.186 million tonnes [48]. Typically, 220–370 kg of GGBFS is generated per ton of produced iron [49]. The used SHA is secondary waste generated from the combustion of sunflower husks, used as an alternative energy source, by an edible oil production company (720 tonnes per year) and a thermal and electrical plant (240 tonnes per year) in the Autonomous Province of Vojvodina—the northern region of the Republic of Serbia [46,50]. Considering the national cement production of 2.73 million tonnes [51], this approach creates the potential to partially substitute conventional binders with local materials, while simultaneously reducing SHA landfilling by its valorisation, thus lowering CO_2 emissions and transportation costs.

The presented study was designed to assess the influence of SHA content and curing conditions on the AAM binder. The SHA content was varied as 15%, 25%, and 35% SHA by mass of GGBFS, based on the reviewed literature [30,32,41], and the results of preliminary investigations. The w/b ratio and GGBFS content were kept constant. Microstructure of the binder was assessed on paste samples by Fourier-transform infrared spectroscopy (FTIR) and thermogravimetric analysis (TGA), after 2, 7 and 28 days of curing at ambient and elevated temperatures (65 °C). Workability and compressive strength were tested on mortar samples. Compressive strength was also tested after 7 and 28 days of curing at two different temperatures. For the optimal mix, SHA was also pre-immersed in water for varying durations to assess its effect on workability, compressive strength, and potassium ion leaching. To monitor the leaching of potassium ions, ion chromatography of the SHA solution was conducted at the same time intervals.

2. Experimental Programme

2.1. Materials

To produce AAMs for experimental testing, GGBFS (Figure 1, on the left) supplied by Lafarge, Serbia, was used as a precursor. The GGBFS had a density of $\rho = 2831$ kg/m^3. SHA used as an activator (Figure 1, on the right) was provided by Victoria Oil, Serbia, a company that processes oil crops and produces edible oil. SHA was obtained as a byproduct of thermal treatment of sunflower husks and was used as received from the plant. The specific surface area determined using the Blaine apparatus was S = 517.8 m^2/kg for GGBFS, and S = 610 m^2/kg for SHA. The particle size distribution of GGBFS and SHA is presented in Figure 2. The median particle size (D50) of GGBFS and SHA was 5.25 µm and 10.5 µm, respectively. The chemical compositions of GGBFS and SHA obtained by X-ray fluorescence (XRF) spectroscopy are presented in Table 1. Quartz sand was used as an aggregate.

Table 1. Chemical composition of GGBFS and SHA obtained by XRF spectroscopy.

Material	Oxide (%)								
	SiO_2	CaO	Al_2O_3	Fe_2O_3	MgO	SO_3	K_2O	Na_2O	LOI
GGBFS	38.69	37.19	9.51	0.47	10.52	2.17	0.83	0.41	0.90
SHA	1.75	14.29	0.59	0.21	10.46	13.53	38.00	0.07	10.45



Figure 1. GGBFS and SHA used in the study.

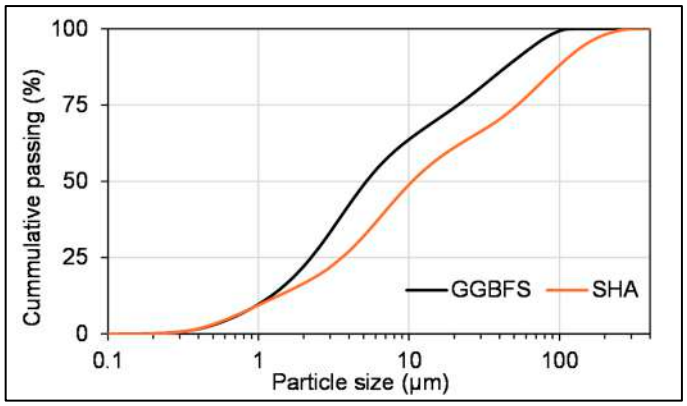


Figure 2. Particle size distribution of GGBFS and SHA.

X-ray diffraction (XRD) pattern and Fourier-transform infrared (FTIR) spectroscopy spectra of SHA are presented in Figures 3 and 4, respectively. The XRD analysis showed strong peaks of arcanite (A), sylvite (S), calcite (C), chamosite (CH) and magnesium oxide (M), and less pronounced peaks of quartz (Q), lime (L) and hematite (H). The presence of arcanite can be confirmed by high peaks at the wavelengths 1110 cm^{-1} and 617 cm^{-1}, in the FTIR spectra of SHA. The absorption bands at 1401 cm^{-1} and 881 cm^{-1} represent C-O symmetric stretching and out-of-plane bending vibrations, respectively.

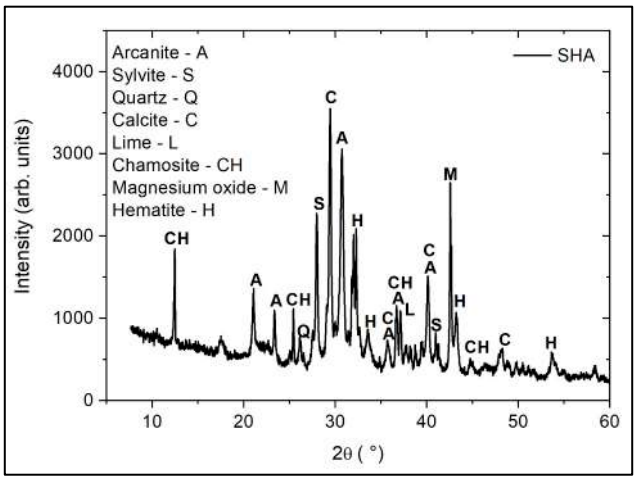


Figure 3. XRD pattern of SHA.

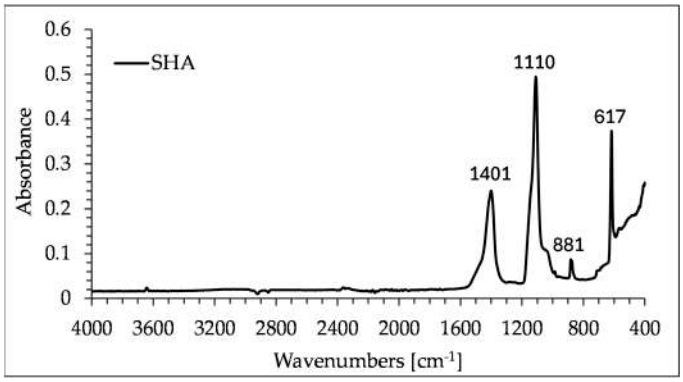


Figure 4. FTIR spectra of SHA.

2.2. Mix Design

Mortar mixes were designed with constant GGBFS content, while SHA content was varied: 15, 25 and 35 wt% GGBFS. All mixes had a w/b ratio of 0.45, and the binder was calculated as the sum of the precursor and the soluble fraction of the SHA, assuming that the entire potassium oxide content was dissolved and contributed to the alkali activation. The mass of the soluble SHA content was previously determined by dissolving SHA in water. The aggregate-to-binder ratio was 3, with the undissolved fraction of SHA included in the total aggregate mass. The mass proportions of the individual fractions were adopted in accordance with those used for a standard cement mortar. Paste mixes were prepared with the same material ratios, with the omission of the aggregates. A detailed mix design is provided in Table 2. The mixtures were labelled based on their composition. The paste mixtures were designated as P15, P25, and P35—the letter "P" denotes pastes, while the numbers 15, 25, and 35 represent the added SHA content wt% GGBFS. Similarly, the letter "M" denotes mortar mixtures, following the same numerical convention, resulting in designations such as M15, M25, and M35.

Table 2. Mix design of paste and mortar mixes.

Mix	GGBFS (g)	SHA (g)	SHA′ (g)	SHA″ (g)	Water (g)	Quartz Sand Fraction (mm)			
						0.008–0.16 (g)	0.16–0.5 (g)	0.5–1.0 (g)	1.0–2.0 (g)
Pastes									
P15	400	60	27	33	192	-	-	-	-
P25	400	100	45	55	200	-	-	-	-
P35	400	140	63	77	208	-	-	-	-
Mortars									
M15	400	60	27	33	192	277	139	416	416
M25	400	100	45	55	200	285	142	427	427
M35	400	140	63	77	208	292	146	438	438

SHA′—SHA dissolved in water; SHA″—mass of SHA undissolved in water.

2.3. Methods

2.3.1. Mixing, Sample Casting and Curing

The reference mixing procedure involved using dry SHA, without prior immersion of SHA in water. In this procedure, GGBFS and SHA were manually dry-mixed and added to aggregates. Three solid components were then manually homogenised, after which they were added to water and mixed in the mixer at high speed for five minutes. The same procedure was followed for paste preparation, but without the addition of the aggregate. Additionally, several procedures were applied, varying the time of immersion

of SHA in water, to assess the influence of pre-dissolution of alkalis (primarily potassium) from SHA on the workability and compressive strength of the obtained mortars. The first step in these procedures was to immerse the SHA and keep it in the water for a different period. The GGBFS and aggregates were dry-mixed and then mixed with SHA and water suspension immediately (0 h) and after 1, 6, and 24 h of immersion. The mixing procedures for assessing the influence of activator preparation on mortar properties are summarised in Table 3. Procedures are marked as Mx,y where x denotes the SHA content in the mix chosen for testing, based on the optimal workability and compressive strength performance. Duration of SHA immersion in water is denoted by y.

Table 3. Mixing procedures for assessing the influence of activator preparation on the mortar properties.

Procedure	Step 1: Immersion	Step 2: Dry-Mixing, Manual	Step 3: Mixing, Manual	Step 4: Mixer
Mx,0 h	SHA immersed just before binder mixing	GGBFS + aggregate	GGBFS + aggregate + SHA suspension	GGBFS + aggregate + SHA suspension
Mx,1 h	SHA was immersed in water for 1 h			
Mx,6 h	SHA was immersed in water for 6 h	GGBFS + aggregate	GGBFS + aggregate + SHA suspension	GGBFS + aggregate + SHA suspension
Mx,24 h	SHA was immersed in water for 24 h			

The mortar samples were cast in prism metal moulds (40 × 40 × 160 mm) and kept in sealed polymeric films to prevent moisture loss for 24 h. Paste samples for testing microstructure were cast in metal moulds with dimensions 5 × 5 × 60 mm and also cured sealed.

The influence of elevated temperature curing was assessed on the mortar mixes with different SHA content, used dry, without immersion in water. After 24 h in moulds, samples were subjected to two different curing regimes. One set of samples was demoulded and cured at an ambient temperature (TA). In contrast, the other set was cured in moulds for 5 days at 65 °C (T65) and then demoulded and cured at ambient temperature until the day of testing, to investigate the influence of curing at elevated temperature on the compressive strength at 7 and 28 days. The two regimes were conducted for samples that were tested for microstructure analysis (TGA and FTIR) and compressive strength at 7 and 28 days. Samples tested at 2 days of age were not subjected to the elevated temperature. Summarised curing regimes are given in Table 4.

Table 4. Curing regimes of paste and mortar samples.

Day of Testing	Curing Regime	First 24 h	5 Days	Until the Day of Testing
2, 7, 28	TA	sealed, ambient temperature		
7, 28	T65	sealed, ambient temperature	sealed, 65 °C	sealed, ambient temperature

2.3.2. Testing Procedures

Phase Composition and Reaction Products

Phase composition in pastes was analysed using thermogravimetric analysis (TGA) and Fourier-transform infrared (FTIR) spectroscopy. TGA was performed on pastes, using the Labsys evo DTA/DSC1150 (Setaram, Geneva, Switzerland). To prepare samples, the paste prisms were crushed into powder and dried in an oven for two hours at 65 °C, and

then immediately tested. Approximately 30 mg of the sample was heated from 30 °C to 1000 °C, with a constant heating rate of 10 °C/min, in an argon atmosphere. The samples were tested at 2, 7 and 28 days of age, according to the curing regimes described in Table 4. FTIR spectroscopy was conducted on paste samples at 2, 7 and 28 days of age. The analysis was conducted using a mobile Alpha Bruker Optics (BRUKER OPTICS, Ettlingen, Germany) FTIR device in ATR (Attenuated Total Reflection) mode, with a diamond as the crystal. The wavenumber range was between 400 and 4000 cm^{-1}. The obtained spectra were analysed using the integrated OPUS software, version 7.2, developed by BRUKER.

Workability and Compressive Strength

The workability of mortar mixes was tested by the flow table test, in accordance with the standard procedure described in SRPS EN 1015-3:1999 [52]. The compressive strength of mortar mixes was tested after 2, 7 and 28 days, in accordance with SRPS EN 196-1:2017 [53].

The Influence of Immersion Time on SHA Dissolution

The influence of the immersion time on SHA dissolution was analysed by monitoring the pH of the SHA solution and by analysing the potassium leaching. The alkalinity of the SHA solution was measured after immersion of the SHA in water to resemble the different mixing procedures given in Table 3. The water-to-SHA ratio was the same as that for the mortar chosen for optimal performance. After the immersion, the solutions were filtered, and their pH values were measured by pH meter Edge HI2020-02 (Hanna Instruments, Woonsocket, RI, USA). The dependence of the potassium leaching on the described immersion times of SHA was quantified by an ion chromatograph, Thermo Scientific DIONEX ICS-5000+ (Thermo Fisher Scientific Inc., Waltham, MA, USA), by dissolving 20 g of SHA in 200 mL of water.

The graphical representation of the experiment design is presented in Figure 5.

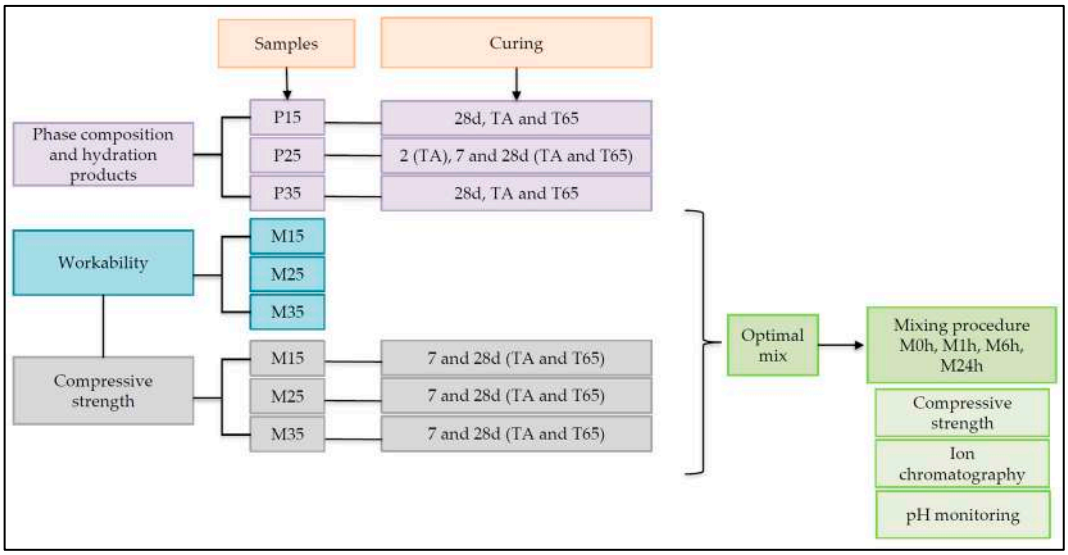


Figure 5. Flowchart of the experiment design.

3. Results and Discussion

3.1. Phase Composition and Reaction Products

The FTIR analysis of pastes with different SHA content after 28 days of curing at the two described regimes is presented in Figure 6. The influence of the curing duration and regime on the FTIR spectra is shown in Figure 7, for the samples with 25% of SHA. The distinct absorbance bands in all tested samples are 3389/3398 cm^{-1}, 1641 cm^{-1},

1401–1412 cm^{-1}, 1104–1109 cm^{-1}, in the range between 1000 and 800 cm^{-1}, 941/942 cm^{-1}, 615 cm^{-1} and 430/441 cm^{-1}. The band at 871 cm^{-1} is present in the spectra of samples tested at an early age (2 and 7 days).

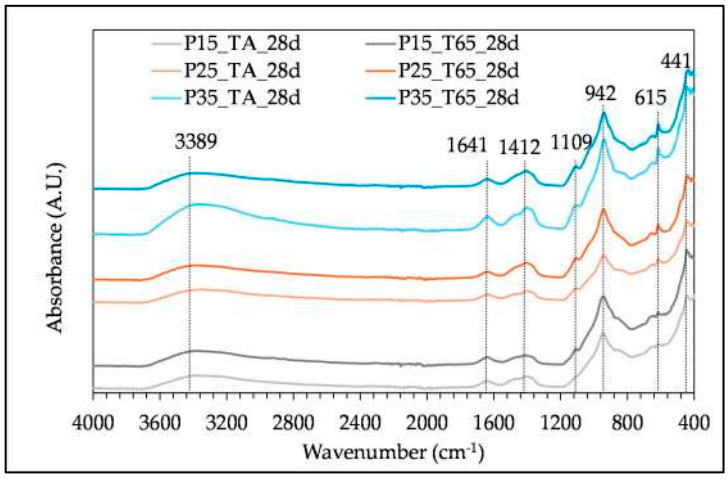


Figure 6. FTIR spectra of paste samples with different SHA content cured at two different regimes, tested at 28 days.

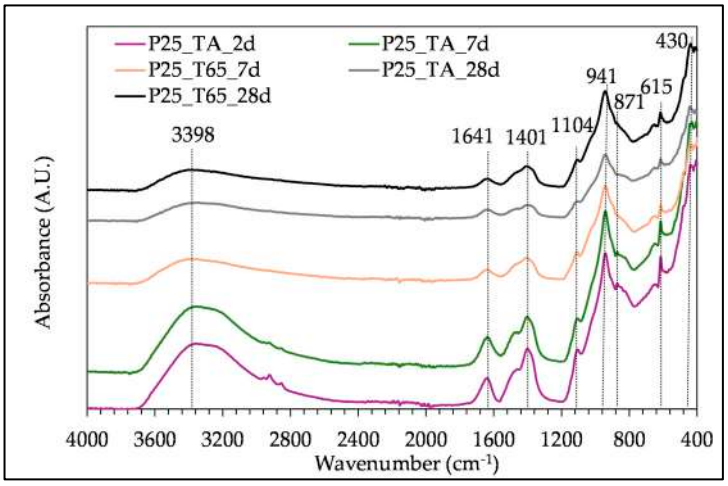


Figure 7. FTIR spectra of paste with 25% of SHA, cured at two different regimes, tested at 2, 7 and 28 days.

The absorbance bands at 3389/3398 cm^{-1} and 1641 cm^{-1} correspond to the O-H stretching and bending vibrations, respectively. They can be seen in all tested samples and present weakly bonded water [54].

The wavelengths 1401 cm^{-1} and 1412 cm^{-1} indicate the C-O asymmetric stretching vibration. The absorption band at 871 cm^{-1} corresponds to C-O out-of-plane bending vibrations [45,55]. The peak at 1109 cm^{-1} (Figure 6) represents symmetric stretching vibrations associated with the sulphate group SO_4^{2-} [46], and it increases with the addition of the SHA. This is due to the presence of arcanite in SHA, seen in the XRD pattern (Figure 3) and FTIR spectra (Figure 4, peaks at 1110 cm^{-1} and 617 cm^{-1}) [47]. The main band at 941 cm^{-1} represents asymmetrical Si-O-Si(Al) stretching vibrations [54,55] and Si-O-M (M-alkali or alkali earth metal) [56]. This absorption band is related to the SiQ^n, where n = 2, according to [55]. The band indicates calcium alumino silicate hydrate (C-A-S-H) and calcium silicate hydrate (C-S-H). Some research on BFS alkali-activation by CHA and SHA combined FTIR with SEM/EDS analysis, concluding that these gels could also

incorporate potassium (C-(K)-A-S-H gels) [42,45]. The addition of SHA resulted in higher peak intensity and integrated peak area of the main band representing C-A-S-H and C-S-H gels, as presented in Table 5 for the samples P15, P25, P35, cured at the T65 regime. When observing the influence of curing regime on the FTIR spectra, the band around 940 cm^{-1} tends to be sharper with an increase in curing temperature (Figure 6).

Table 5. Peak intensities and integrated peak areas at the main absorbance band for the samples P15, P25 and P35, cured at T65, tested at 28 days of age.

Sample	Absolute Peak Intensity * (a.u.)	Integrated Peak Area * (a.u.)
P15_T65	0.164	25.541
P25_T65	0.175	24.826
P35_T65	0.179	25.764

* FTIR spectra of the samples P15_T65, P25_T65, and P35_T65, from which the peak intensities and areas were obtained, are presented in Figure S1, Figure S2, and Figure S3 of the Supplementary Materials, respectively.

The absorption bands at 615 cm^{-1} are Al-O and Mg-O bending modes, possibly from hydrotalcite [57]. Peaks in the range 430–441 cm^{-1} are characteristic of flexural vibrations of Si-O-Si [58].

TG curves and differential thermogravimetric (DTG) curves of the tested pastes are presented in Figures 8–10. All samples exhibit DTG peaks commonly formed in the alkali-activated slag systems, such as peaks indicating C-S-H, C-A-S-H and hydrotalcite [59], which is in line with FTIR analysis and research on SSA and SHA slurries [44]. The peak between 30 °C and 200 °C corresponds to the loss of structurally unbound water from the C-S-H. This peak overlaps with the one between 140 °C and 240 °C, associated with the dehydration of C-A-S-H [60]. In studies on OBA [31,32] and ABA [39] activated slags, these peaks are also attributed to the C-(K)-S-H and C-(K)-A-S-H gels. The formation of hydrotalcite is confirmed by the peak between 300 °C and 400 °C [31,32]. However, due to its layered structure, it is possible that it contributes to the peak around 200 °C [61]. The peaks between 440 °C and 550 °C [23] and 600 °C and 700 °C [41,60] present decomposition of $CaCO_3$.

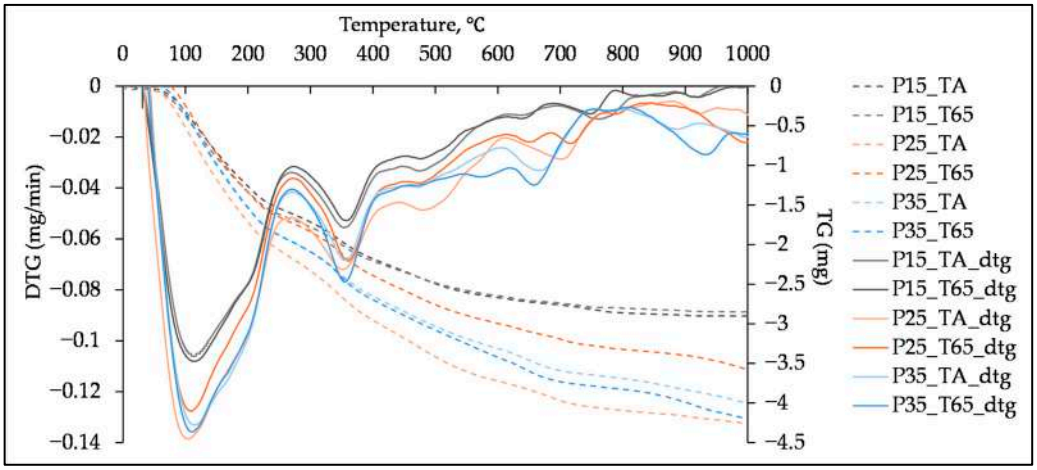


Figure 8. TG and DTG curves of paste samples with different SHA content cured at two different regimes, tested at 28 days.

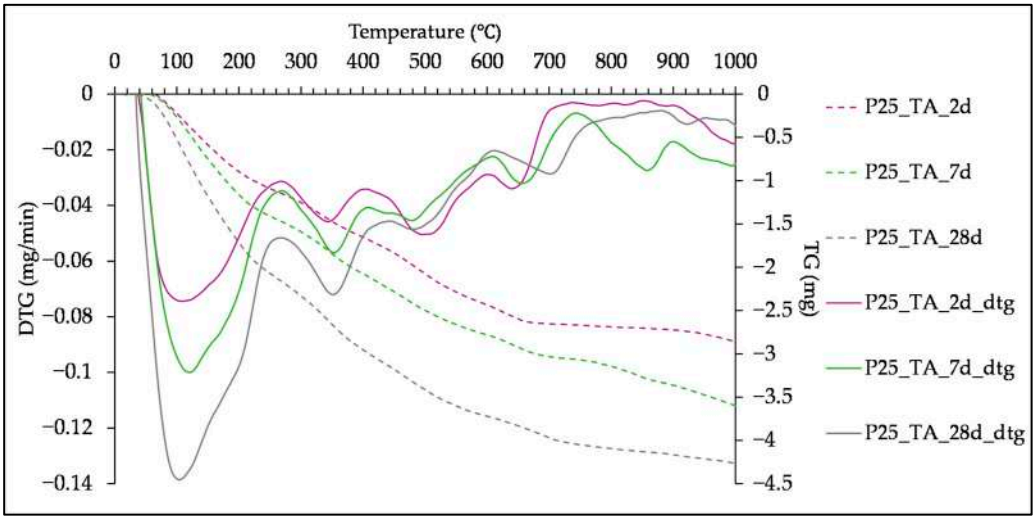


Figure 9. TG and DTG curves of paste with 25% of SHA, cured at TA, tested at 2, 7 and 28 days.

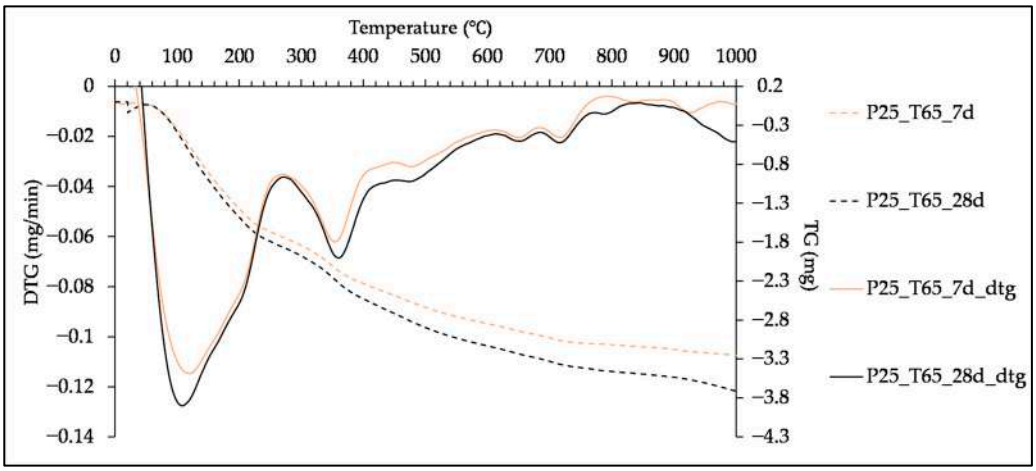


Figure 10. TG and DTG curves of paste with 25% of SHA, cured at T65, tested at 7 and 28 days.

The influence of SHA content and curing regimes after 28 days of curing can be seen in Figure 8. Table 6 presents the mass loss percentages for peaks representing main hydration products, C-A-S-H, C-S-H (Peak 1) and hydrotalcite (Peak 2). The intensity of the peaks and mass loss percentage of samples cured at T65 increase with the addition of SHA, as it was observed by FTIR analysis (Table 5), suggesting the formation of more hydration products due to the higher alkali content [31,32]. Although the difference in the Peak 1 between the TA and T65 curing regimes for samples P15 and P35 appears small—and the T65 regime even shows slightly sharper peaks—the mass loss results indicate otherwise. Specifically, the TGA analysis shows that the T65-cured samples exhibit lower mass loss in the region associated with C-A-S-H and C-S-H decomposition, suggesting that less hydration products are formed under the T65 regime. In DSC curves of the sample P25, it is clearly visible that the T65 curing regime resulted in less prominent peaks 1 and 2 than TA, as confirmed by higher mass loss of the samples cured at TA (6.790 and 2.055) compared to those at T65 (5.458 and 1.767). The exception was sample P35, cured at T65; it had higher Peak 2, compared to the sample cured at TA. However, this could be the consequence of analysing a very small sample of heterogeneous material.

Table 6. Mass loss from 30 to 240 °C and from 300 to 400 °C of samples P15, P25 and P35, after 28 days of curing at TA and T65 regimes.

	Mass Loss (%)					
Sample	P15		P25		P35	
Curing regime	TA	T65	TA	T65	TA	T65
Peak 1 (30–240 °C)	4.777	3.386	6.790	5.458	6.145	5.942
Peak 2 (300–400 °C)	1.472	0.963	2.055	1.767	1.563	1.851

The influence of curing duration at the TA and T65 curing regimes is presented for the pastes with 25% of SHA, in Figures 9 and 10, respectively. The longer curing time led to higher mass loss and sharpening of the characteristic peaks, which is also explained by the increase in hydration degree through time [30,31]. Curing at 65 °C altered only the peak formation at 7 days, while it did not have a positive effect on the gel formation after 28 days of curing, as mentioned in the previous section.

3.2. Workability

Mortar mixes after the flow table test are presented in Figure 11. All mixes exhibited homogeneity with no segregation or bleeding. The increase in SHA content (i.e., increased content of fine particles) has led to an increased demand for water, which has resulted in a decrease in workability [62]. This was reflected in the moderate decrease in slump flow, shown in Figure 12.

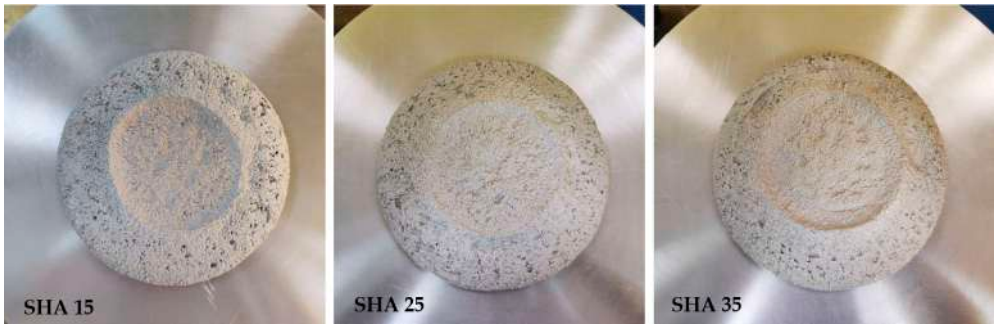


Figure 11. Mortar mixes after the flow table test.

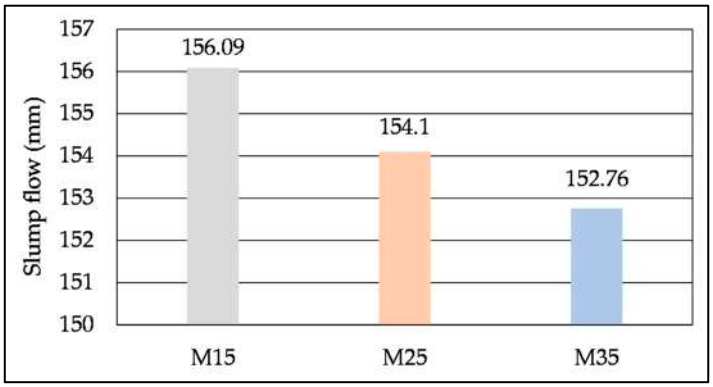


Figure 12. Slump flow of mortar mixes with different SHA content.

3.3. Compressive Strength—Influence of Curing Regime and SHA Content

Examples of hardened samples before and after testing are presented in Figures 13 and 14. Curing regime T65 altered the development of 7-day compressive strengths for all SHA contents (Figure 15). Curing at elevated temperatures was also found to be beneficial for

early strength development in other studies with different biomass ashes [30–32]. Contrary to expectations and findings in the literature on AAMs with biomass ashes [33], higher compressive strength at 28 days was obtained for the TA than the T65 curing regime (Figure 16). Although the reduced strength with the T65 regime was not pronounced, it may be attributed to the accelerated reaction kinetics induced by elevated temperatures. This rapid reaction can lead to the early formation of dense hydration products, which inhibit further gel development by limiting ion diffusion and promoting microstructural inhomogeneity [63]. An additional explanation found in the literature is that exposure to elevated curing temperatures can lead to significant water evaporation, thereby reducing the amount of free water available for subsequent hydration reactions [64,65]. The interpretation of the compressive strength results is supported by TGA analysis (Figure 8 and Table 6), which shows that more hydration products are formed at 28 days under the TA curing regime compared to T65. Overall, elevated-temperature curing appears to be more effective in enhancing early-age strength. After 7 days, mortars M15, M25, and M35 achieved 89%, 91%, and 98% of their respective 28-day compressive strengths, respectively.



Figure 13. Example of hardened samples before testing of the compressive strength.



Figure 14. Example of a sample cross-section after testing of the compressive strength.

The increase in SHA content has led to an increase in compressive strength at both 7 and 28 days (Figures 15 and 16), due to the formation of more hydration products; however, mixes M25 and M35 at 28 days exhibited essentially the same strengths. This can also be explained by the fast initial reaction in the presence of more alkalis, hindering the development of compressive strength at 28 days. The increase in SHA content also resulted in higher DTG and FTIR peaks, representing the C-S-H, C-A-S-H, and possibly C-(K)-S-H and C-(K)-A-S-H gel (Figure 8, Tables 5 and 6). The formation of the gels could also be altered by the CaO in the SHA [44]. The increase in biomass ash content was followed by higher

compressive strengths in the works of other authors as well [32,41,43]. The contribution to compressive strength could also be attributed to the filler effect of undissolved SHA [41,44]. However, Moraes Pinheiro et al. [32] found that the filler effect in the OBA-activated slag was negligible, compared to the OBA contribution to the slag activation.

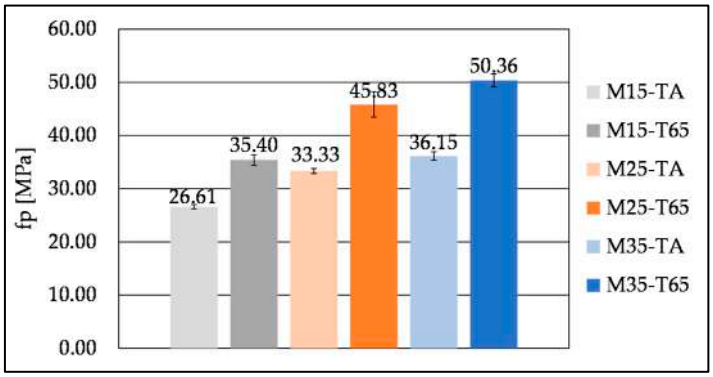


Figure 15. Compressive strength of mortar mixes with different SHA content cured at TA and T65 curing regimes, tested at 7 days.

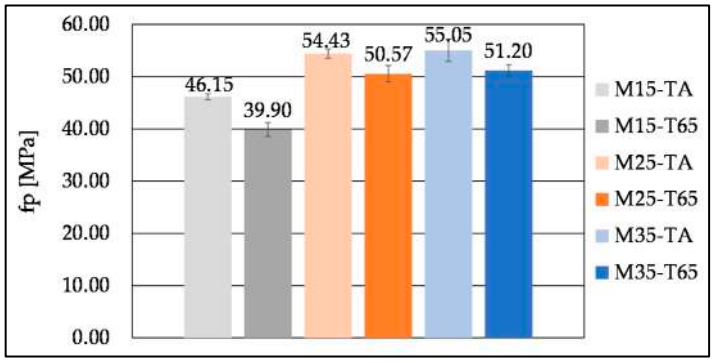


Figure 16. Compressive strength of mortar mixes with different SHA content cured at TA and T65 curing regime, tested at 28 days.

The 7-day compressive strengths obtained under the T65 curing regime are comparable to or higher than those reported in the literature. The highest 7-day compressive strengths previously reported were 38.38 MPa for mortars with the addition of 25% of OBA [32] and 45.2 MPa for those incorporating almond biomass ash [40], both cured at 65 °C, for 7 days. Mortar samples in this study achieved 35.4 MPa (15% SHA), 45.83 MPa (25% SHA) and 50.36 MPa (35% SHA) (Figure 15). Furthermore, the published data shows that mortars activated with 10, 20 and 30 wt% BFS of HBA exhibited 28-day compressive strength from 22.1 MPa to 26.8 MPa, at ambient temperature, corresponding to 1.7 M, 1.9 M, and 2.0 M NaOH, and 1.8 M, 2.0 M and 2.2 M KOH molarities, respectively [41]. In another study, mortars based on BFS and CHA yielded 29.9 MPa and 40.9 MPa after 7 and 28 days of curing at ambient temperature and 95% RH, respectively [45]. Under the TA curing regime, the results of this research show similar compressive strengths for 7 days of curing (Figure 15) and significantly higher 28-day compressive strengths by up to 15 MPa (Figure 16).

Although strength development depends on multiple factors, such as the chemical composition of the biomass ash and GGBFS, mix design, and curing regime, the comparison leads to the conclusion that the use of SHA in alkali activation can result in compressive strengths of the same order of magnitude as those reported in the literature for other biomass ashes.

3.4. Influence of Mixing Procedure on Workability and Compressive Strength of the Mix M25

This section provides insight into the effect of the duration of SHA immersion in water before mixing the M25 mortar. This mix was selected as optimal based on the slump flow and compressive strength.

Figure 17 presents the slump flow for the mortars mixed with no immersion of the SHA (M25), followed by the immersion procedures described in Table 3 (M25/0 h, M25/1 h, M25/6 h and M25/24 h). Mixes with prolonged immersion times of up to 6 h resulted in a decrease in slump flow, while the mix M25/24 h exhibited a higher slump than the mix M25/6 h.

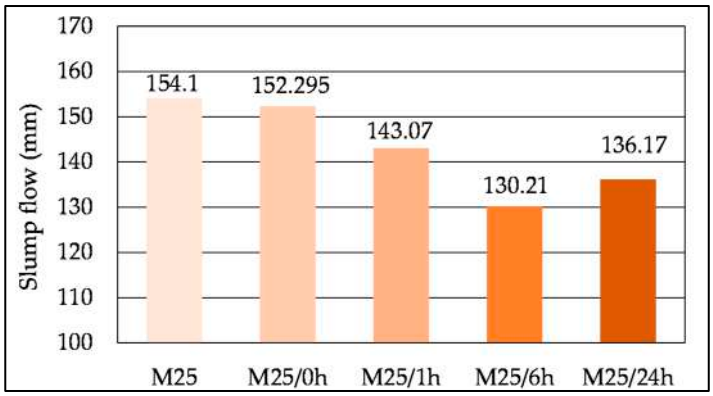


Figure 17. Influence of the mixing procedure on the workability of the mix M25.

The compressive strengths (Figure 18) of the mixes M25, M25/0 h, and M25/1 h after 7 days of ambient curing were similar. Mixes M25/6 h and M25/24 h showed a mild increase in compressive strength. However, the difference between the lowest and the highest was approximately 5 MPa.

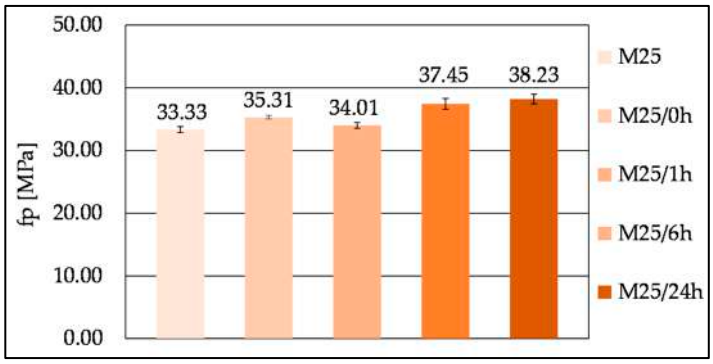


Figure 18. Influence of the mixing procedure on the compressive strength of the mix M25 at 7 days of age.

The increase in compressive strength can be attributed to the higher dissolution degree of potassium from SHA over time, confirmed by ion chromatography (Figure 19), thus increasing the pH (Figure 20) and altering alkali activation. Furthermore, the immersion time up to 24 h and the pH value of the suspension have a strong linear correlation (R^2 = 0.9561). Although the pH of the SHA suspension increases with immersion time, this does not significantly improve the compressive strength (up to 14.7%). Therefore, SHA can be used as received, without previous dissolution in water. This considerably simplifies its potential practical application, as the binder can be produced by pre-mixing solid components and subsequently adding water.

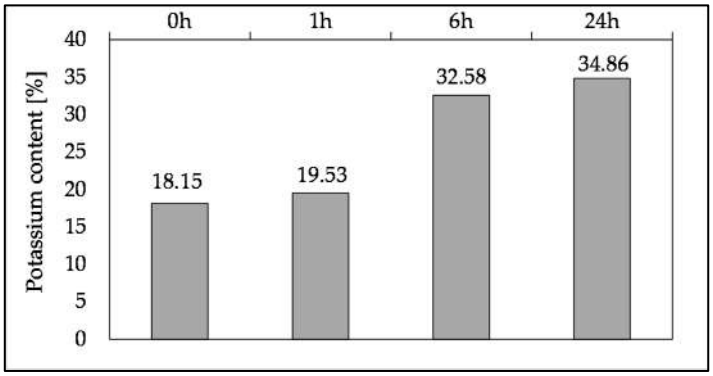


Figure 19. Potassium content in the leachate of SHA after different immersion times.

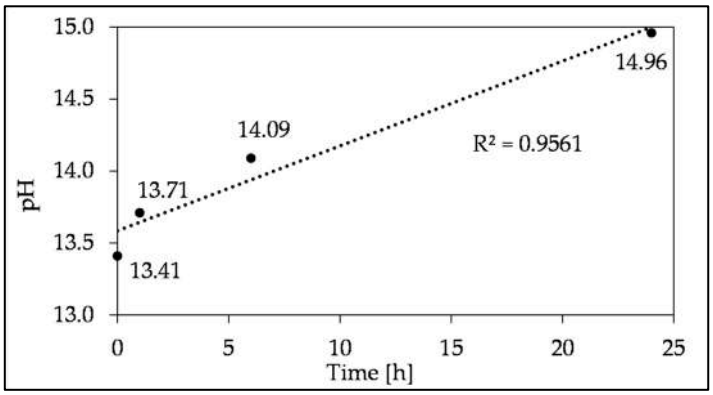


Figure 20. Changes in the alkalinity of the SHA suspension depending on the duration of the SHA immersion in water.

4. Conclusions

This paper presents a study on the optimisation of an alkali-activated binder based on locally available secondary waste materials. It investigates the potential of using SHA as an alternative activator for GGBFS. The influence of SHA content, curing regime (ambient and elevated temperature), and mixing procedure was evaluated on paste and mortar mixes activated with 15%, 25%, and 35% SHA by mass of GGBFS. The following conclusions can be drawn:

- FTIR and TGA analyses confirmed that the reaction between SHA and GGBFS results in the formation of C-S-H and C-A-S-H gels, characteristic of alkali-activation of slag.
- Increasing the SHA content leads to a minor reduction in workability and alters gel formation, consequently increasing compressive strength.
- Curing at 65 °C promotes early strength development (attaining 89–98% of 28-day compressive strength) but results in lower 28-day compressive strength compared to ambient curing.
- Immersion of SHA in water before mixing enhances the dissolution of potassium ions and results in higher compressive strength up to 14.7%, depending on the immersion duration; however, it negatively impacts workability.
- The highest 28-day compressive strength of 55 MPa (25% SHA) is attained with minimal technological requirements, without SHA pretreatment and dissolution in water before mixing, cured at ambient temperature. This is 15 MPa higher than reported in the literature, highlighting the novelty for mortar mixes with similar component materials, mix designs, and curing conditions.

The presented research demonstrated that SHA can be directly used, as received, without prior dissolution, which contributes to the cost-effectiveness of the studied AAM.

This enables one-part alkali-activation through the pre-mixing of solids, followed by water addition during the binder mixing. Therefore, the production of AAMs is significantly simplified, enhancing their potential practical applicability compared to chemical hydroxide activators. The results are a base for the development of alkali-activated concrete mixes, and future research will focus on their durability properties. In addition to technical performance, the utilisation of the locally sourced SHA supports the principles of the circular economy, enhances the sustainability of the proposed waste-based binder, and promotes the valorisation of alternative energy sources by-products.

Supplementary Materials: The following supporting information can be downloaded at: https://www.mdpi.com/article/10.3390/buildings15234210/s1, Figure S1: FTIR spectra of the sample P15, cured at the T65 regime; Figure S2: FTIR spectra of the sample P25, cured at the T65 regime; Figure S3: FTIR spectra of the sample P35, cured at the T65 regime.

Author Contributions: Conceptualization, O.B., S.D. and M.S.; methodology, O.B., S.D. and M.S.; validation, O.B., S.D., S.V. and M.S.; formal analysis, O.B.; investigation, O.B. and S.D.; resources, O.B., S.D., S.V. and M.S.; data curation, O.B. and S.D.; writing—original draft preparation, O.B. and S.D.; writing—review and editing, O.B., S.D., S.V. and M.S.; visualisation, O.B.; supervision, S.D. and M.S.; funding acquisition, M.S. All authors have read and agreed to the published version of the manuscript.

Funding: This research has been supported by the Ministry of Science, Technological Development and Innovation, Republic of Serbia (Contract No. 451-03-137/2025-03/200156 and 451-03-137/2025-03/200134) and the Faculty of Technical Sciences, University of Novi Sad, through project "Scientific and Artistic Research Work of Researchers in Teaching and Associate Positions at the Faculty of Technical Sciences, University of Novi Sad 2025" (No. 01-50/295).

Data Availability Statement: The original contributions presented in this study are included in the article and Supplementary Materials. Further inquiries can be directed to the corresponding author.

Conflicts of Interest: The authors declare no conflicts of interest.

References

1. Marsh, A.; Dillon, T.; Bernal, S. Cement and Concrete Decarbonisation Roadmaps—A Meta-Analysis within the Context of the United Kingdom. *RILEM Tech. Lett.* **2023**, *8*, 94–105. [CrossRef]
2. United Nations Environment Programme. *Building Materials and the Climate: Constructing a New Future*; United Nations Environment Programme: Paris, France, 2023; ISBN 978-92-807-4064-6.
3. Habert, G.; Miller, S.A.; John, V.M.; Provis, J.L.; Favier, A.; Horvath, A.; Scrivener, K.L. Environmental Impacts and Decarbonization Strategies in the Cement and Concrete Industries. *Nat. Rev. Earth Env.* **2020**, *1*, 559–573. [CrossRef]
4. Provis, J.L. Alkali-Activated Materials. *Cem. Concr. Res.* **2018**, *114*, 40–48. [CrossRef]
5. Ramagiri, K.K.; Kar, A. Environmental Impact Assessment of Alkali-Activated Mortar with Waste Precursors and Activators. *J. Build. Eng.* **2021**, *44*, 103391. [CrossRef]
6. Provis, J.L.; Van Deventer, J.S.J. Geopolymers and Other Alkali-Activated Materials. In *Lea's Chemistry of Cement and Concrete*; Butterworth-Heinemann: Oxford, UK, 2019; pp. 779–805. ISBN 978-0-08-100773-0.
7. Provis, J.L. Green Concrete or Red Herring?–Future of Alkali-Activated Materials. *Adv. Appl. Ceram.* **2014**, *113*, 472–477. [CrossRef]
8. Komkova, A.; Habert, G. Environmental Impact Assessment of Alkali-Activated Materials: Examining Impacts of Variability in Constituent Production Processes and Transportation. *Constr. Build. Mater.* **2023**, *363*, 129032. [CrossRef]
9. Pol Segura, I.; Ranjbar, N.; Juul Damø, A.; Skaarup Jensen, L.; Canut, M.; Arendt Jensen, P. A Review: Alkali-Activated Cement and Concrete Production Technologies Available in the Industry. *Heliyon* **2023**, *9*, e15718. [CrossRef] [PubMed]
10. Segura, I.P.; Luukkonen, T.; Yliniemi, J.; Sreenivasan, H.; Damø, A.J.; Jensen, L.S.; Canut, M.; Kantola, A.M.; Telkki, V.-V.; Jensen, P.A. Comparison of One-Part and Two-Part Alkali-Activated Metakaolin and Blast Furnace Slag. *J. Sustain. Metall.* **2022**, *8*, 1816–1830. [CrossRef]
11. Luukkonen, T.; Abdollahnejad, Z.; Yliniemi, J.; Kinnunen, P.; Illikainen, M. One-Part Alkali-Activated Materials: A Review. *Cem. Concr. Res.* **2018**, *103*, 21–34. [CrossRef]

12. Alnahhal, M.F.; Kim, T.; Hajimohammadi, A. Waste-Derived Activators for Alkali-Activated Materials: A Review. *Cem. Concr. Compos.* **2021**, *118*, 103980. [CrossRef]
13. Mendes, B.C.; Pedroti, L.G.; Vieira, C.M.F.; Marvila, M.; Azevedo, A.R.G.; Franco De Carvalho, J.M.; Ribeiro, J.C.L. Application of Eco-Friendly Alternative Activators in Alkali-Activated Materials: A Review. *J. Build. Eng.* **2021**, *35*, 102010. [CrossRef]
14. Mohapatra, S.S.; Mishra, J.; Nanda, B.; Patro, S.K. A Review on Waste-Derived Alkali Activators for Preparation of Geopolymer Composite. *Mater. Today Proc.* **2022**, *56*, 440–446. [CrossRef]
15. Vassilev, S.V.; Baxter, D.; Andersen, L.K.; Vassileva, C.G. An Overview of the Composition and Application of Biomass Ash. Part 1. Phase–Mineral and Chemical Composition and Classification. *Fuel* **2013**, *105*, 40–76. [CrossRef]
16. Munawar, M.A.; Khoja, A.H.; Naqvi, S.R.; Mehran, M.T.; Hassan, M.; Liaquat, R.; Dawood, U.F. Challenges and Opportunities in Biomass Ash Management and Its Utilization in Novel Applications. *Renew. Sustain. Energy Rev.* **2021**, *150*, 111451. [CrossRef]
17. Odzijewicz, J.I.; Wołejko, E.; Wydro, U.; Wasil, M.; Jabłońska-Trypuć, A. Utilization of Ashes from Biomass Combustion. *Energies* **2022**, *15*, 9653. [CrossRef]
18. Marathe, S.; Sadowski, Ł. Developments in Biochar Incorporated Geopolymers and Alkali Activated Materials: A Systematic Literature Review. *J. Clean. Prod.* **2024**, *469*, 143136. [CrossRef]
19. Bernal, S.A.; Rodríguez, E.D.; Kirchheim, A.P.; Provis, J.L. Management and Valorisation of Wastes through Use in Producing Alkali-activated Cement Materials. *J. Chem. Technol. Biotechnol.* **2016**, *91*, 2365–2388. [CrossRef]
20. Ahmad, Z.; Qureshi, M.I.; Ahmad, F.; El Ouni, M.H.; Asghar, M.Z.; Ghazouani, N. Effect of Macro Synthetic Fiber (MSF) on the Behavior of Conventional Concrete and the Concrete Containing e-Waste Aggregates. *Mater. Struct.* **2025**, *58*, 234. [CrossRef]
21. Bernal, S.A.; Rodríguez, E.D.; de Gutiérrez, R.M.; Provis, J.L. Performance at High Temperature of Alkali-Activated Slag Pastes Produced with Silica Fume and Rice Husk Ash Based Activators. *Mater. Construcción* **2015**, *65*, e049. [CrossRef]
22. Mejía, J.M.; de Gutiérrez, R.M.; Montes, C. Rice Husk Ash and Spent Diatomaceous Earth as a Source of Silica to Fabricate a Geopolymeric Binary Binder. *J. Clean. Prod.* **2016**, *118*, 133–139. [CrossRef]
23. Moraes, J.C.B.; Font, A.; Soriano, L.; Akasaki, J.L.; Tashima, M.M.; Monzó, J.; Borrachero, M.V.; Payá, J. New Use of Sugar Cane Straw Ash in Alkali-Activated Materials: A Silica Source for the Preparation of the Alkaline Activator. *Constr. Build. Mater.* **2018**, *171*, 611–621. [CrossRef]
24. Gomonsirisuk, K.; Thavorniti, P. Use of Water Glass from Rice Husk and Bagasse Ashes in the Preparation of Fly Ash Based Geopolymer. *KEM* **2019**, *798*, 364–369. [CrossRef]
25. Villaquirán-Caicedo, M.A. Studying Different Silica Sources for Preparation of Alternative Waterglass Used in Preparation of Binary Geopolymer Binders from Metakaolin/Boiler Slag. *Constr. Build. Mater.* **2019**, *227*, 116621. [CrossRef]
26. Tchakouté, H.K.; Rüscher, C.H.; Kong, S.; Ranjbar, N. Synthesis of Sodium Waterglass from White Rice Husk Ash as an Activator to Produce Metakaolin-Based Geopolymer Cements. *J. Build. Eng.* **2016**, *6*, 252–261. [CrossRef]
27. Tchakouté, H.K.; Rüscher, C.H.; Kong, S.; Kamseu, E.; Leonelli, C. Geopolymer Binders from Metakaolin Using Sodium Waterglass from Waste Glass and Rice Husk Ash as Alternative Activators: A Comparative Study. *Constr. Build. Mater.* **2016**, *114*, 276–289. [CrossRef]
28. Bernal, S.A.; Rodríguez, E.D.; Mejia De Gutiérrez, R.; Provis, J.L.; Delvasto, S. Activation of Metakaolin/Slag Blends Using Alkaline Solutions Based on Chemically Modified Silica Fume and Rice Husk Ash. *Waste Biomass Valor.* **2012**, *3*, 99–108. [CrossRef]
29. Tong, K.T.; Vinai, R.; Soutsos, M.N. Use of Vietnamese Rice Husk Ash for the Production of Sodium Silicate as the Activator for Alkali-Activated Binders. *J. Clean. Prod.* **2018**, *201*, 272–286. [CrossRef]
30. Font, A.; Soriano, L.; de Moraes Pinheiro, S.M.; Tashima, M.M.; Monzó, J.; Borrachero, M.V.; Payá, J. Design and Properties of 100% Waste-Based Ternary Alkali-Activated Mortars: Blast Furnace Slag, Olive-Stone Biomass Ash and Rice Husk Ash. *J. Clean. Prod.* **2020**, *243*, 118568. [CrossRef]
31. Font, A.; Soriano, L.; Moraes, J.C.B.; Tashima, M.M.; Monzó, J.; Borrachero, M.V.; Payá, J. A 100% Waste-Based Alkali-Activated Material by Using Olive-Stone Biomass Ash (OBA) and Blast Furnace Slag (BFS). *Mater. Lett.* **2017**, *203*, 46–49. [CrossRef]
32. de Moraes Pinheiro, S.M.; Font, A.; Soriano, L.; Tashima, M.M.; Monzó, J.; Borrachero, M.V.; Payá, J. Olive-Stone Biomass Ash (OBA): An Alternative Alkaline Source for the Blast Furnace Slag Activation. *Constr. Build. Mater.* **2018**, *178*, 327–338. [CrossRef]
33. Alonso, M.M.; Gascó, C.; Morales, M.M.; Suárez-Navarro, J.A.; Zamorano, M.; Puertas, F. Olive Biomass Ash as an Alternative Activator in Geopolymer Formation: A Study of Strength, Radiology and Leaching Behaviour. *Cem. Concr. Compos.* **2019**, *104*, 103384. [CrossRef]
34. Soriano, L.; Font, A.; Borrachero, M.V.; Monzó, J.M.; Payá, J.; Tashima, M.M. Biomass Ashes to Produce an Alternative Alkaline Activator for Alkali-Activated Cements. *Mater. Lett.* **2022**, *308*, 131198. [CrossRef]
35. Peys, A.; Rahier, H.; Pontikes, Y. Potassium-Rich Biomass Ashes as Activators in Metakaolin-Based Inorganic Polymers. *Appl. Clay Sci.* **2016**, *119*, 401–409. [CrossRef]
36. Balo, A.M.; Rahier, H.; Mobili, A.; Katsiki, A.; Fagel, N.; Chinje, U.M.; Njopwouo, D. Metakaolin-Based Inorganic Polymer Synthesis Using Cotton Shell Ash as Sole Alkaline Activator. *Constr. Build. Mater.* **2018**, *191*, 1011–1022. [CrossRef]

37. Adesanya, E.; Perumal, P.; Luukkonen, T.; Yliniemi, J.; Ohenoja, K.; Kinnunen, P.; Illikainen, M. Opportunities to Improve Sustainability of Alkali-Activated Materials: A Review of Side-Stream Based Activators. *J. Clean. Prod.* **2021**, *286*, 125558. [CrossRef]
38. Cheah, C.B.; Part, W.K.; Ramli, M. The Hybridizations of Coal Fly Ash and Wood Ash for the Fabrication of Low Alkalinity Geopolymer Load Bearing Block Cured at Ambient Temperature. *Constr. Build. Mater.* **2015**, *88*, 41–55. [CrossRef]
39. Soriano, L.; Font, A.; Tashima, M.M.; Monzó, J.; Borrachero, M.V.; Payá, J. One-Part Blast Furnace Slag Mortars Activated with Almond-Shell Biomass Ash: A New 100% Waste-Based Material. *Mater. Lett.* **2020**, *272*, 127882. [CrossRef]
40. Soriano, L.; Font, A.; Tashima, M.M.; Monzó, J.; Borrachero, M.V.; Bonifácio, T.; Payá, J. Almond-Shell Biomass Ash (ABA): A Greener Alternative to the Use of Commercial Alkaline Reagents in Alkali-Activated Cement. *Constr. Build. Mater.* **2021**, *290*, 123251. [CrossRef]
41. Omur, T.; Kanat, D.; Kabay, N. Innovative Use of Hazelnut Shell Ash as an Alkali Activator: A Comparative Analysis with Commercial Activators. *J. Build. Eng.* **2024**, *90*, 109466. [CrossRef]
42. Zhu, Z.; Li, X.; Liu, R.; Wang, Z.; Zhang, H.; Zhao, D.; Bai, J.; Chen, M.; Li, W. Workability and Environmental Evaluation of Using Sunflower Stalk Ash as an Alkali Activator with Blast Furnace Slag and Black Rice Hull Ash to Prepare Geopolymer Grouts. *Waste Biomass Valor.* **2025**, *16*, 1609–1626. [CrossRef]
43. Zhu, Z.; Xu, X.; Liu, R.; Liu, P.; Tang, H.; Gong, Y.; Zhang, C.; Li, X.; Liu, Y.; Bai, J.; et al. Feasibility Study of Highly Alkaline Biomass Ash to Activate Alkali-Activated Grouts. *Constr. Build. Mater.* **2023**, *393*, 132067. [CrossRef]
44. Zhu, Z.; Zhang, C.; Liu, R.; Li, S.; Wang, M. Sunflower Straw Ash as an Alternative Activator in Alkali-Activated Grouts: A New 100% Waste-Based Material. *Ceram. Int.* **2023**, *49*, 32308–32312. [CrossRef]
45. Lima, F.S.; Gomes, T.C.F.; Moraes, J.C.B. Effect of Coffee Husk Ash as Alkaline Activator in One-Part Alkali-Activated Binder. *Constr. Build. Mater.* **2023**, *362*, 129799. [CrossRef]
46. Bedov, O.; Andabaka, A.; Draganić, S. Turning Agricultural Biomass Ash into a Valuable Resource in the Construction Industry—Exploring the Potential of Industrial Symbiosis. *Buildings* **2025**, *15*, 273. [CrossRef]
47. Nikolov, A.; Kostov, V.; Petrova, N.; Tsvetanova, L.; Vassilev, S.V.; Titorenkova, R. Sunflower Shells Biomass Fly Ash as Alternative Alkali Activator for One-Part Cement Based on Ladle Slag. *Ceramics* **2025**, *8*, 79. [CrossRef]
48. World Steel Association. *Steel Statistical Yearbook 2022*; World Steel Association: Brussels, Belgium, 2022.
49. Shen, H.; Forssberg, E. An Overview of Recovery of Metals from Slags. *Waste Manag.* **2003**, *23*, 933–949. [CrossRef] [PubMed]
50. Draganić, S.; Šupić, S.; Laban, M.; Malešev, M.; Bulatović, V.; Lukić, I.; Bukvić, O. Agricultural Biomass Ash as a Circular Building Material: Connecting Agriculture and Construction Industry. In *Creating a Roadmap Towards Circularity in the Built Environment*; Springer: Cham, Switzerland, 2023; pp. 225–236. ISBN 978-3-031-45979-5.
51. Statistical Office of the Republic of Serbia. *Industrial Production by Products*; Statistical Office of the Republic of Serbia: Belgrade, Serbia, 2024.
52. *SRPS EN 1015-3:2008*; Methods of Test for Mortar for Masonry. Determination of Consistence of Fresh Mortar (by Flow Table). Institute for Standardization of Serbia: Belgrade, Serbia, 2008.
53. *SRPS EN 196-1: 2017*; Methods of Testing Cement-Part 1: Determination of Strength. Institute for Standardization of Serbia: Belgrade, Serbia, 2017.
54. Ghorbani, S.; Stefanini, L.; Sun, Y.; Walkley, B.; Provis, J.L.; De Schutter, G.; Matthys, S. Characterisation of Alkali-Activated Stainless Steel Slag and Blast-Furnace Slag Cements. *Cem. Concr. Compos.* **2023**, *143*, 105230. [CrossRef]
55. Lecomte, I.; Henrist, C.; Liégeois, M.; Maseri, F.; Rulmont, A.; Cloots, R. (Micro)-Structural Comparison between Geopolymers, Alkali-Activated Slag Cement and Portland Cement. *J. Eur. Ceram. Soc.* **2006**, *26*, 3789–3797. [CrossRef]
56. Sun, Y.; De Lima, L.M.; Rossi, L.; Jiao, D.; Li, Z.; Ye, G.; De Schutter, G. Interpretation of the Early Stiffening Process in Alkali-Activated Slag Pastes. *Cem. Concr. Res.* **2023**, *167*, 107118. [CrossRef]
57. Ismail, I.; Bernal, S.A.; Provis, J.L.; San Nicolas, R.; Hamdan, S.; van Deventer, J.S.J. Modification of Phase Evolution in Alkali-Activated Blast Furnace Slag by the Incorporation of Fly Ash. *Cem. Concr. Compos.* **2014**, *45*, 125–135. [CrossRef]
58. Li, B.; Sun, Q.; Chen, X.; Xu, Z.; Yang, L. Preparation and Microstructure Analysis of Alkali-Activated Ground Granulated Blast Furnace Slag-Steel Slag Grouting Materials. *Case Stud. Constr. Mater.* **2024**, *20*, e03235. [CrossRef]
59. Shi, Z.; Shi, C.; Wan, S.; Li, N.; Zhang, Z. Effect of Alkali Dosage and Silicate Modulus on Carbonation of Alkali-Activated Slag Mortars. *Cem. Concr. Res.* **2018**, *113*, 55–64. [CrossRef]
60. Bílek, V.; Švec, J.; Másilko, J.; Sedlačík, M.; Materak, K.; Wieczorek, A.; Koniorczyk, M.; Hajzler, J.; Kucharczyková, B. Comparison of Thermogravimetry Response of Alkali-Activated Slag and Portland Cement Pastes after Stopping Their Hydration Using Solvent Exchange Method. *J. Therm. Anal. Calorim.* **2025**, *150*, 1013–1037. [CrossRef]
61. Ben Haha, M.; Le Saout, G.; Winnefeld, F.; Lothenbach, B. Influence of Activator Type on Hydration Kinetics, Hydrate Assemblage and Microstructural Development of Alkali Activated Blast-Furnace Slags. *Cem. Concr. Res.* **2011**, *41*, 301–310. [CrossRef]
62. Sona, S.; Sangeetha, S.P. Eco-Friendly Alternative Activators Derived from Industrial Wastes for the Sustainable Production of Two-Part Geopolymer Concrete at Low Cost. *Constr. Build. Mater.* **2025**, *467*, 140374. [CrossRef]

63. Bakharev, T.; Sanjayan, J.G.; Cheng, Y.-B. Effect of Elevated Temperature Curing on Properties of Alkali-Activated Slag Concrete. *Cem. Concr. Res.* **1999**, *29*, 1619–1625. [CrossRef]
64. Aliabdo, A.A.; Abd Elmoaty, A.E.M.; Emam, M.A. Factors Affecting the Mechanical Properties of Alkali Activated Ground Granulated Blast Furnace Slag Concrete. *Constr. Build. Mater.* **2019**, *197*, 339–355. [CrossRef]
65. Collins, F.; Sanjayan, J.G. Microcracking and Strength Development of Alkali Activated Slag Concrete. *Cem. Concr. Compos.* **2001**, *23*, 345–352. [CrossRef]

Disclaimer/Publisher's Note: The statements, opinions and data contained in all publications are solely those of the individual author(s) and contributor(s) and not of MDPI and/or the editor(s). MDPI and/or the editor(s) disclaim responsibility for any injury to people or property resulting from any ideas, methods, instructions or products referred to in the content.